TURBULENT FLAME PROPAGATION CHARACTERISTICS OF HIGH HYDROGEN CONTENT FUELS

CONTRACT: DE-FE0004555

REPORT TYPE: FINAL REPORT

REPORTING PERIOD START DATE: OCTOBER 1, 2010

REPORTING PERIOD END DATE: SEPTEMBER 30, 2014

AUTHORS: PROF. JERRY M. SEITZMAN**,** PROF. TIMOTHY C. LIEUWEN

DATE REPORT WAS ISSUED: DECEMBER 2014

NAME AND ADDRESS OF SUBMITTING ORGANIZATION:

GEORGIA INSTITUTE OF TECHNOLOGY

SCHOOL OF AEROSPACE ENGINEERING

270 FERST DRIVE

ATLANTA, GA, 30332

DISCLAIMER

Abstract

This final report describes the results of an effort to better understand turbulent flame propagation, especially at conditions relevant to gas turbines employing fuels with syngas or hydrogen mixtures. Turbulent flame speeds were measured for a variety of hydrogen/carbon monoxide (H_2/CO) and hydrogen/methane (H_2/CH_4) fuel mixtures with air as the oxidizer. The measurements include global consumption speeds ($S_{T,GC}$) acquired in a turbulent jet flame at pressures of 1-10 atm and local displacement speeds ($S_{T,LD}$) acquired in a low-swirl burner at atmospheric pressure. The results verify the importance of fuel composition in determining turbulent flame speeds. For example, different fuel-air mixtures having the same unstretched laminar flame speed ($S_{L,0}$) but different fuel compositions resulted in significantly different $S_{T,GC}$ for the same turbulence levels (u'). This demonstrates the weakness of turbulent flame speed correlations based simply on $u'/S_{L,0}$. The results were analyzed using a steady-steady leading points concept to explain the sensitivity of turbulent burning rates to fuel (and oxidizer) composition. Leading point theories suggest that the premixed turbulent flame speed is controlled by the flame front characteristics at the flame brush leading edge, or, in other words, by the flamelets that advance farthest into the unburned mixture (the so-called leading points). For negative Markstein length mixtures, this is assumed to be close to the maximum stretched laminar flame speed ($S_{L,\max}$) for the given fuel-oxidizer mixture. For the $S_{T,GC}$ measurements, the data at a given pressure were well-correlated with an $S_{L,\max}$ scaling. However the variation with pressure was not captured, which may be due to non-quasi-steady effects that are not included in the current model. For the $S_{T,LD}$ data, the leading points model again faithfully captured the variation of turbulent flame speed over a wide range of fuel-compositions and turbulence intensities. These results provide evidence that the leading points model can provide useful predictions of turbulent flame speed over a wide range of operating conditions and flow geometries.

TABLE OF CONTENTS

Introduction

The purpose of this report is to present and analyze turbulent flame speed data acquired. The first section gives an overview of some of the global consumption turbulent flame speed data acquired by Venkateswaran [20]. The goal of this section is to present in more detail some of the background work that laid the foundation for the development of the low swirl burner facility and the acquisition of localized flow and flame measurements for validation of the leading points model. This section will present global consumption speed $S_{T,GC}$ measurements with a focus on the effects of fuel composition and pressure. The data are also analyzed using the leading points model. Some of the deficiencies of the leading points model are noted from this data, and an attempt to understand these deficiencies in terms of non-quasi-steady effects on the flame is presented. The next section presents measurements and analysis of local displacement turbulent flame speed data acquired in the LSB. These measurements were acquired to supplement the global consumption measurements, and, thus, were acquired at similar operating conditions. In addition, this data is also analyzed using the leading points model to see how this model works on data acquired from a different experimental configuration.

Leading points concepts can be used to develop an inequality for scaling the turbulent flame speed that is similar to the classical Damköhler turbulent flame speed scaling [5], except the parameter arising from the analysis is the maximum stretched laminar flame speed, $S_{L,max}$ [19]. In certain situations this inequality can be replaced by an equality. For example, because the mixtures investigated in this work are thermodiffusively unstable, $S_{L,0}$ is a repelling point since a positively curved perturbation on a flat flame will grow with increasing curvature and correspondingly increasing flame speeds. In fact, it can be rigorously shown that $S_{L,max}$ is a steady-state attracting point for constant density flames with positively curved wrinkles [19]. As such, if the turbulent eddies evolve over a time scale that is slow relative to that required for the leading points to be attracted to the $S_{L,max}$ point, the equality seen below can be used:

$$\frac{S_T}{S_{L,max}} = 1 + \frac{u'_{LP}}{S_{L,max}} \tag{1}$$

Another important caveat is that $S_{L,max}$ is itself a frequency dependent quantity. In other words, the augmentation of the laminar burning velocity by stretch decreases, while the extinction stretch rate increases, for unsteady flames [10]. Thus, there are two important non-quasi-steady effects which influence this scaling, one related to the geometry of the turbulent flame brush, and the other related to the internal flame structure.

Overview

This section describes measurements and correlations of turbulent consumption speeds, $S_{T,GC}$, of hydrogen and carbon monoxide (H_2:CO) fuel mixtures, with

a focus on elevated pressure data. Turbulent consumption speed data were obtained at mean flow velocities and turbulence intensities of $30 < U_0 < 50$ m/s and $5 < u'_{rms}/S_{L,0} < 30$, respectively, for H_2:CO mixtures ranging from 30-90% H_2 by volume from 1-10 atm. Experiments were conducted where the mixture equivalence ratio, ϕ, was adjusted at each fuel composition to have nominally the same unstretched laminar flame speed, $S_{L,0}$. In comparing two blends with the same composition, $S_{L,0}$ value, and flow conditions, the 5 and 10 atm data have $S_{T,GC}$ values that are consistently about 1.8 and 2.2 times larger than the 1 atm data, respectively. These data are also correlated with the scaling law derived from quasi-steady leading points concepts using detailed kinetics calculations of highly stretched flames. For a given pressure, these scalings do an excellent job in scaling data obtained across the H_2:CO fuel composition and fuel/air range. However, the pressure sensitivities are not captured by this scaling. This pressure sensitivity may be more fundamentally a reflection of the non-quasi-steady nature of the flame leading points. In support of this argument, the spread in the data can largely be correlated with the ratio of a chemical time scale to a flow time scale.

Background

This section analyzes the scaling relation as well as coupled pressure and fuel effects. There are limited data of this kind in the literature. Turbulent consumption speed measurements of $\phi = 0.9$ CH_4/air were reported by Kobayashi et al. [14]. It was concluded that $S_{T,GC}/S_{L,0}$ increased with pressure due to $S_{L,0}$ decreasing but that $S_{T,GC}$ itself was independent of pressure. Kitagawa et al. [13] reported measurements of turbulent flame speeds of H_2/air mixtures at pressures ranging from 1-5 atm. They found that pressure had an influence on $S_T/S_{L,0}$ through the pressure effect on $S_{L,0}$, however, the influence on S_T is unclear. Daniele et al. [6] report $S_{T,GC}$ measurements of H_2:CO mixtures for pressures of 1-20 atm at 623 K. They found that $S_{T,GC}/S_{L,0}$ increased with pressure at each given H_2:CO ratio and $u'_{rms}/S_{L,0}$ value.

Methods

Image Processing

The image processing methodology has been extensively documented in [19], but is briefly overviewed here. Global consumption speeds were calculated, whose key measurement input is the progress variable surface area, A_f.

Digital images of the flame emission were captured with a 16-bit intensified charge-coupled device (ICCD) camera. Line-of-sight images of the flame were obtained over five seconds and time-averaged. To estimate the time-averaged flame brush location from the line-of-sight images, a three-point Abel deconvolution scheme [7] was used. The axial distribution of the centerline intensity was then fit to a Gaussian curve, from which the location of the maximum intensity

was identified. This point is associated with the most probable location of the flame, and defined as the $\langle c \rangle = 0.5$ progress variable contour. The estimated uncertainty in identifying this point is 1-2%. Straight lines are then drawn from this point to the two flame anchoring points and rotated about the line of symmetry to generate a cone; i.e., the "angle method" [14, 2, 17]. The overall uncertainty in the $S_{T,GC}$ value is estimated to be 3%.

Stretch Sensitivity Calculations

Stretch sensitivity calculations were performed for the mixtures investigated in Table 1. Stretch sensitivities were calculated using an opposed flow calculation of two premixed flames with a nozzle separation distance of 20 mm using the OPPDIF [12] module in CHEMKIN. An arc length continuation method was used to determine the extinction point. From these calculations, various stretched properties of the mixture were extracted. In this work, the displacement laminar flame speed is considered, determined from the minimum velocity just upstream of the reaction zone as suggested by Wu and Law [21].

Results:Global Consumption Speeds

Experimental Conditions

Measurements of $S_{T,GC}$ were obtained at 1, 5, and 10 atm as a function of $u'_{rms}/S_{L,0}$ using a 12 mm diameter Bunsen burner. Data were acquired at mean flow velocities from 20-50 m/s and volumetric H_2:CO ratios ranging from 30:70-90:10, keeping $S_{L,0}$ and reactant temperature fixed at 34 cm/s and 300 K, respectively. $S_{L,0}$ was kept nominally constant by adjusting the stoichiometry at each H_2:CO ratio. $S_{L,0}$ estimates were determined using the PREMIX module [11] in CHEMKIN with the Davis H_2/CO mechanism for H_2:CO mixtures [8]. The parameter ranges explored in this study along with the symbol type and color scheme are summarized in Table 1. Figure 1 summarizes where the measured data are located on the Borghi-Peters diagram [3, 16]. The data fall within the thin reaction zones regime ($1 < Ka < 100$), implying that Kolmogorov eddies may enter the preheat zone but are still too large to enter the reaction zone where they may lead to quenching [16].

H_2:CO Sweeps at Constant $S_{L,0}$

In this section, $S_{T,GC}$ data acquired at 1, 5 and 10 atm are reported. As described earlier, data were acquired for mixtures where the H_2:CO ratio and equivalence ratio were simultaneously adjusted to maintain the same mixture $S_{L,0}$ of 34 cm/s.

Figure 2 plots $S_{T,GC}$ as a function of u'_{rms} normalized by $S_{L,0}$ for the range of conditions reported in Table 1. Note that the 5 atm data were acquired for mean flow velocities of 30 and 50 m/s and the 10 atm data for 30 m/s.

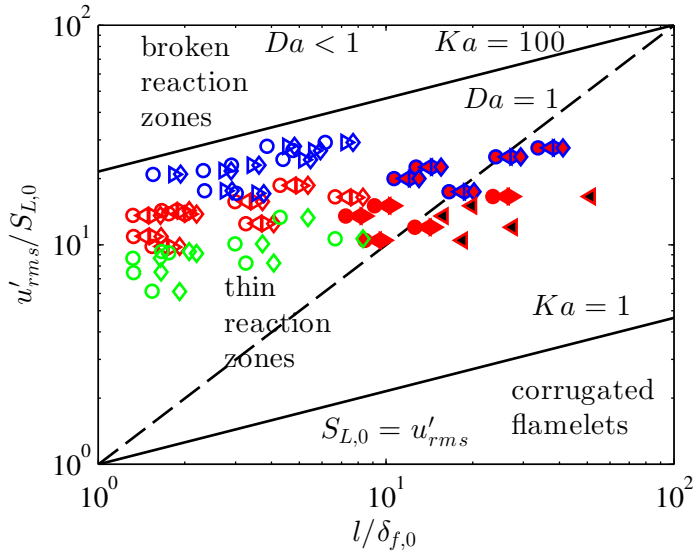

Figure 1: Borghi-Peters diagram showing location of 12 mm burner data points at 1, 5 and 10 atm.

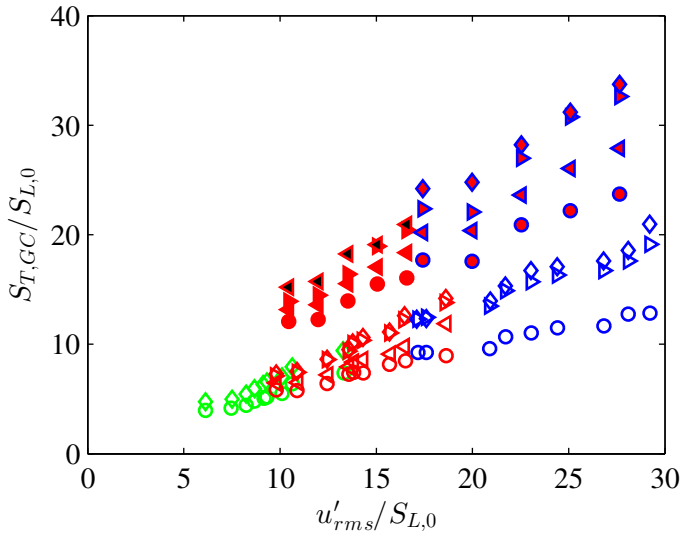

Figure 2: $S_{T,GC}$ as a function of u'_{rms} normalized by $S_{L,0}$ at various mean flow velocities, H_2:CO ratios, and pressures for the 12 mm diameter burner (See Table 1 for the legend of mixture conditions, flow velocities and pressures).

Table 1: Investigated 12 mm burner data set

Parameter	Value (Legend Designation)			
U_0 (m/s)	20 (Green markers) 30 (Red markers) 50 (Blue markers)			
H_2 (%)	30 (○)	50 (◁)	70 (▷)	90 (◇)
ϕ ($p = 1$ atm)	0.61 (no fill)	0.55 (no fill)	0.51 (no fill)	0.48 (no fill)
ϕ ($p = 5$ atm)	0.75 (red fill)	0.68 (red fill)	0.63 (red fill)	0.59 (red fill)
ϕ ($p = 10$ atm)		0.75 (black fill)		

Several important observations can be made from this figure. First, the "fuel effect" is clearly present at the elevated pressure conditions; i.e., different H_2:CO blends at constant $S_{L,0}$ and u'_{rms} have different turbulent flame speeds. Second, it is clear that $S_{T,GC}$ at 5 atm is approximately double its value at 1 atm, and increases slightly further at 10 atm. This increase is quantified in Figure 3, which plots the ratio of $S_{T,GC}$ at 5 and 10 atm to 1 atm for each mixture and mean flow velocity as a function of turbulence intensity. This ratio has values of about 1.8 and 2.2 at 5 and 10 atm, respectively. Note that this is not an $S_{L,0}$ effect, as $S_{L,0}$ is kept fixed at 34 cm/s. The next section describes analysis and discussion of the data.

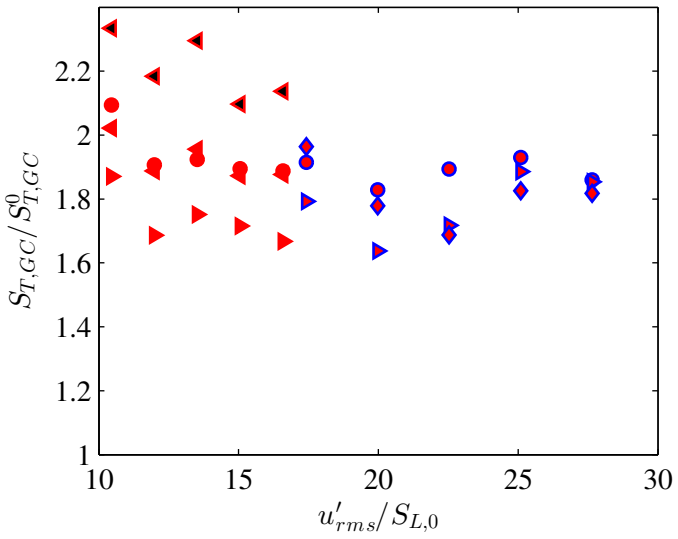

Figure 3: Ratio of $S_{T,GC}$ at 5 and 10 atm to 1 atm across the range of turbulence intensities investigated.

Analysis

In this section, the data presented in Figure 2 are correlated using the steady-state leading points scaling law of Equation 1. Before doing so, it is useful to present pressure effects on the calculated stretch sensitivity of the mixtures investigated. Figure 4 plots the stretch sensitivity of 70:30 H_2:CO mixtures whose $S_{L,0}$ is kept constant at 34 cm/s across the pressures by adjusting the equivalence ratio.

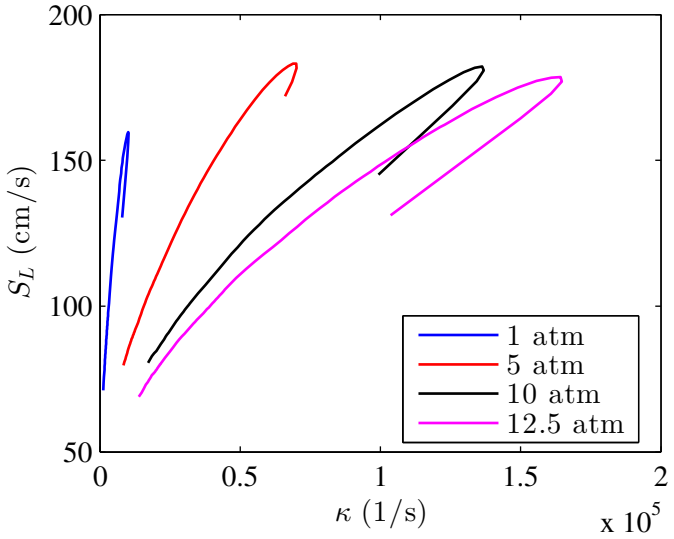

Figure 4: Pressure effect on mixture stretch sensitivity for 70:30 H_2:CO mixtures at constant $S_{L,0}$.

Note from Figure 4 that the extinction stretch rate, κ_{ext}, and the Markstein length, l_M, scale with the pressure. In other words, if the pressure is increased by a factor of 5, the extinction stretch rate and Markstein length increase and decrease by a factor of approximately 5, respectively. This can be explained by the thinning of the flame with pressure. These two effects compensate so that $S_{L,max}$ is relatively insensitive to pressure. In fact, above 5 atm $S_{L,max}$ remains almost constant and actually decreases beyond 12.5 atm.

Similar calculations were performed to normalize the measured turbulent flame speed data, as shown in Figure 5. This figure shows that both the 5 atm and 1 atm data sets collapse quite well individually but that there are systematic differences between them. No similar comparison can be made for the 10 atm data set, since only one composition was examined.

In addition to the 12 mm diameter burner dataset presented in this section, an extensive set of atmospheric pressure consumption speed measurements using a 20 mm diameter burner was also acquired [19]. This normalization produced

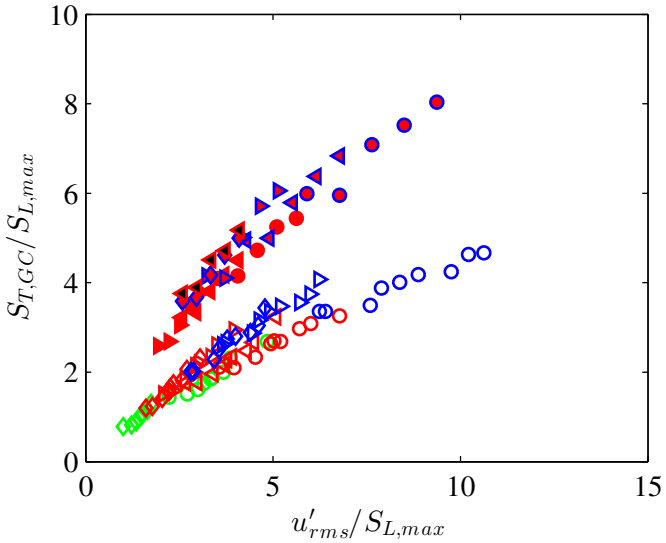

Figure 5: $S_{T,GC}$ as a function of u'_{rms} normalized by $S_{L,max}$ at various mean flow velocities, H_2:CO ratios and pressures using the 12 mm diameter burner (See Table 1 for legend of mixture conditions, flow velocities and pressures).

the interesting result that the 30 m/s CH_4 data did not collapse with the H_2:CO data. However, all constant $S_{L,0}$ data and equivalence ratio sweep data collapse very well.

To summarize, all the data taken consistently show that Equation 1 collapses data across all H_2:CO and equivalence ratio values at a given pressure. However, it does not collapse the 30 m/s CH_4 data nor does it collapse data taken at different pressures. The rest of this section analyzes potential reasons for this and particularly focuses on non-quasi-steady chemistry effects.

In starting this discussion of the data, it is important to note that $S_{L,max}$ is itself not a fundamental property of the mixture. For example, the burning velocity of highly stretched flames is a function of the manner in which the flame is stretched, i.e., by tangential flow straining or curvature, as well as the stretch profile through the flame (manifested by, for example, moderate sensitivities of $S_{L,max}$ or κ_{ext} to the opposed flow nozzle separation distance or velocity profile) [9]. Note that these calculations derive $S_{L,max}$ from a tangentially stretched flame, while the actual flame leading points are curved. Our research group has also performed expanding cylindrical flame and tubular flame computations that indicate that $S_{L,max}$ varies by about 20-40%, depending on the manner in which the flame stretch is applied [1]. In addition, very different $S_{L,max}$ values are obtained when using consumption and displacement based burning velocities [15]. Finally, $S_{L,max}$ is itself a frequency dependent quantity [10]; the steady state values used here are only appropriate if the internal structure

of the leading point is quasi-steady. The rest of this discussion focuses on the non-quasi-steady chemical processes, as the calculations presented next suggest that this is the largest effect.

To investigate this influence, a chemical time scale associated with $S_{L,max}$ was calculated from:

$$\tau_{S_{L,max}} = \frac{\delta_f|_{S_{L,max}}}{S_{L,max}} \tag{2}$$

where $\delta_{f,S_{L,max}}$ is the flame thickness at $S_{L,max}$ and is calculated from:

$$\delta_f = \frac{T_p - T_r}{(dT/dx)_{max}} \tag{3}$$

δ_f The variation in the chemical time scale across H_2:CO mixtures and pressures is shown in Figure 6. The point corresponding to 0% H_2 is the pure CH_4/air case that was used in the constant $S_{L,0}$ studies with the 20 mm burner.

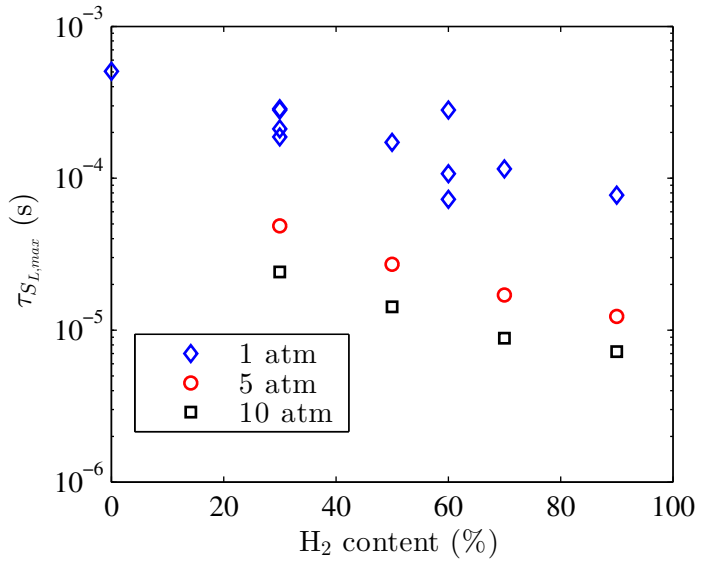

Figure 6: Variation in $\tau_{S_{L,max}}$ as a function of H_2 content for the different mixtures and conditions investigated. 0% H_2 corresponds to the pure CH_4 mixture.

Within the H_2:CO mixtures, $\tau_{S_{L,max}}$ increases by about a factor of 3.5 as the H_2 content is increased from 30% to 90% at 1 atm. The difference between the CH_4 case and the 90:10 H_2:CO mixture is about a factor of 6.5. In addition, for a fixed H_2 content of 30%, there is a factor of 6 reduction in$\tau_{S_{L,max}}$ for a pressure increase from 1 to 5 atm.

Figure 7 plots $S_{T,GC}/S_{L,max}$ as a function of $\tau_{S_{L,max}}/\tau_{flow}$, where $\tau_{flow} = D/U_0$, at two turbulence intensity conditions for the 12 mm burner. Also

shown are power law fits to the data, where the fit parameter, b, is defined by $S_{T,GC}/S_{L,max} \sim \left(\tau_{S_{L,max}}/\tau_{flow}\right)^b$.

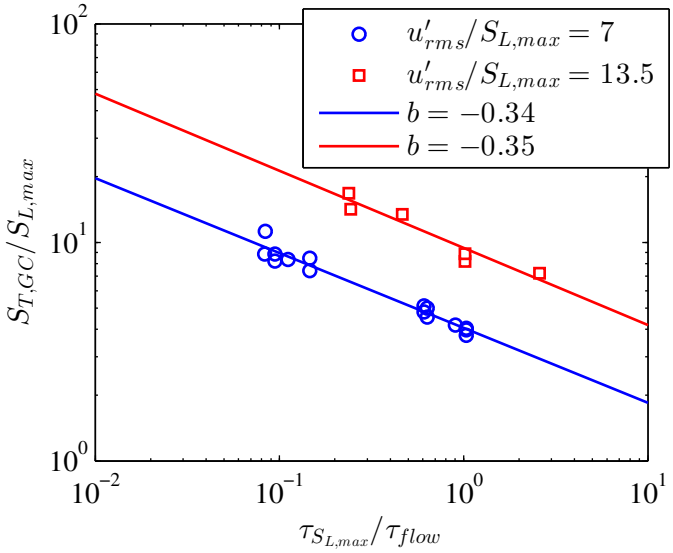

Figure 7: Dependence of $S_{T,GC}/S_{L,max}$ on $\tau_{S_{L,max}}/\tau_{flow}$ at two turbulence intensities $u'_{rms}/S_{L,max} = 7$ and 13.5 for the 12 mm diameter burner. Power law fits with the corresponding slopes are also included.

Note the clear correlation between turbulent flame speed and time scale ratio across the entire range of pressure and fuel composition. Slower chemistry is associated with lower values of the normalized turbulent flame speed, as would be expected, since the effective flame speed of the non-quasi-steady flame is lower than its quasi-steady value. While the time scale ratios are much less than unity (indicating that the chemistry is actually quasi-steady with respect to the large scales), the corresponding ratios calculated using Kolmogorov time scales range from 20-95 for the same data. In other words, significant non-quasi-steady chemistry effects would be expected for small flow length scale-flame interactions.

Similar analysis at other turbulence intensities showed good correlations. In addition, the 1 atm data from the 20 mm burner, shown in Figure **??**, also showed good correlations for the 4 and 10 m/s data. The 30 m/s CH_4 data, however, did not collapse well. Results for the 20 mm diameter burner are presented in Figure 8 for two turbulence intensities. Again, notice the clear decreasing trend of turbulent flame speed values with increasing time scale ratio. In the subsequent section, turbulent local displacement flame speed, $S_{T,LD}$, results obtained using the low swirl burner geometry are presented over a wide range of fuel compositions, mean flow velocities, and turbulence intensities. These results are normalized using the conventional $S_{L,0}$ normalization and then

normalized with $S_{L,max}$ to compare the efficacy of the leading points scaling model for a different burner geometry and flame speed definition.

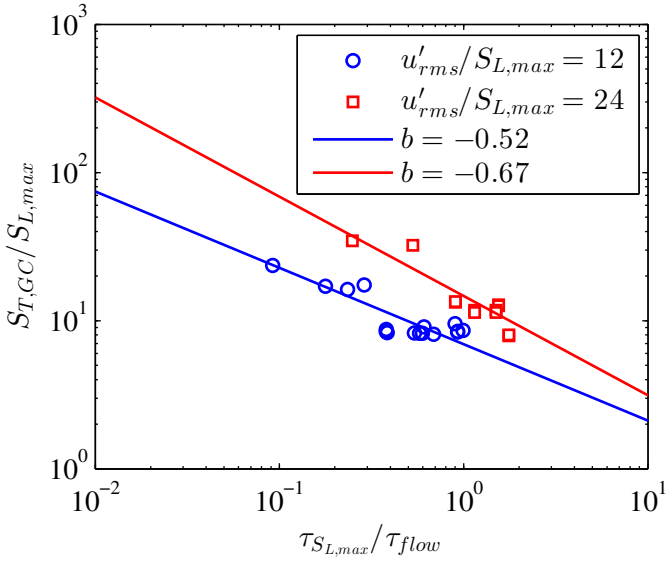

Figure 8: Dependence of $S_{T,GC}/S_{L,max}$ on $\tau_{S_{L,max}}/\tau_{flow}$ at two turbulence intensities $u'_{rms}/S_{L,max} = 12$ and 24 for the 20 mm diameter burner. Power law fits with the corresponding slopes are also included.

Turbulent Local Displacement Flame Speeds

Overview

This section details measurements and correlations of turbulent local displacement speeds, $S_{T,LD}$, of hydrogen - carbon monoxide (H_2:CO) and hydrogen - methane (H_2:CH_4) fuel mixtures. Turbulent local displacement speed data were obtained at mean flow velocities and turbulence intensities of $30 < U_0 < 50$ m/s and $3 < u'_{ax}/S_{L,0} < 12$, respectively, for H_2:CO mixtures ranging from 50-100% H_2 and H_2:CH_4 mixtures from 0-75% H_2 by volume. As for the global consumption measurements, experiments were conducted where the mixture equivalence ratio,ϕ, was adjusted at each fuel composition to have nominally the same unstretched laminar flame speed, $S_{L,0}$, of 34 cm/s. The data are also correlated with the leading points scaling law using detailed kinetics calculations of highly stretched flames.

Results

Experimental Conditions

Measurements of $S_{T,LD}$ were obtained at atmospheric conditions as a function of $u'_{ax}/S_{L,0}$ using a 36 mm diameter LSB. Data were acquired at mean flow velocities from 30-50 m/s, keeping $S_{L,0}$ and reactant temperature fixed at 34 cm/s and 300 K, respectively. $S_{L,0}$ estimates were determined using the PREMIX module [11] in CHEMKIN with the Davis H_2/CO mechanism for H_2:CO mixtures [8] and GRI-Mech 3.0 [18] for CH_4-containing mixtures. Figure 9 summarizes where the measured data are located on the Borghi-Peters diagram [3, 16]. As was true for the 12 mm Bunsen burner, the data fall within the thin reaction zones regime ($1 < Ka < 100$), implying that Kolmogorov eddies may enter the preheat zone but are still too large to enter the reaction zone where they may lead to quenching [16].

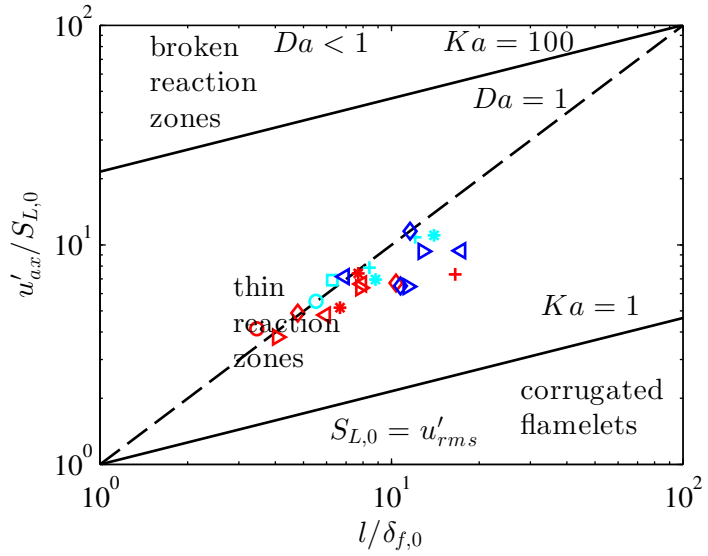

Figure 9: Borghi-Peters diagram showing location of LSB data points. See Figures 10 and 11 for legends.

H_2:CO Sweeps at Constant $S_{L,0}$

In this section, $S_{T,LD}$ data acquired for H_2:CO mixtures are reported. As described earlier, data were acquired for mixtures where the H_2:CO ratio and equivalence ratio were simultaneously adjusted to maintain the same mixture $S_{L,0}$ of 34 cm/s.

Figure 10 plots $S_{T,LD}$ as a function of u'_{ax} normalized by $S_{L,0}$ over a wide range of conditions. Note that the "fuel effect" is clearly present in this data as it

was for the 12 mm Bunsen burner; i.e., different H_2:CO blends at constant $S_{L,0}$ and u'_{ax} have different turbulent flame speeds. For example, at $u'_{ax}/S_{L,0} \approx 7$, the $S_{T,LD}$ values increase by about 50% from the lowest H_2-containing fuel (50:50) to the pure H_2 fuel. Again, for all these data points the equivalence ratio was adjusted to have nominally the same unstretchted laminar flame speed of 34 cm/s.

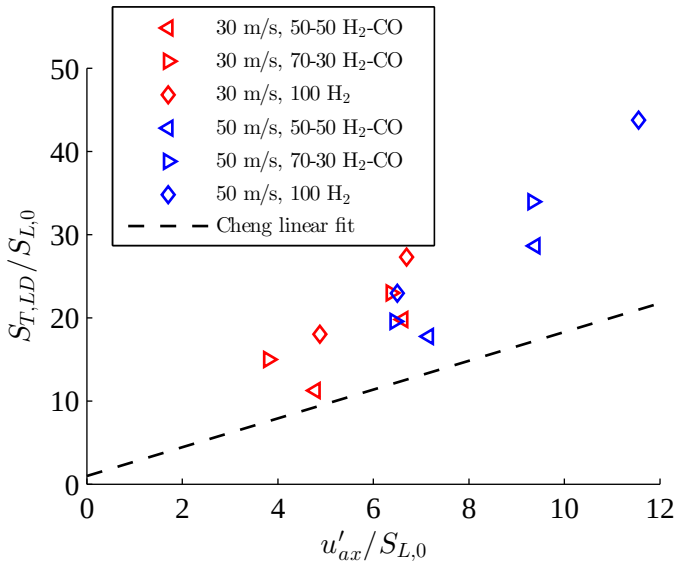

Figure 10: $S_{T,LD}$ as a function of u'_{ax} normalized by $S_{L,0}$ at various mean flow velocities and H_2:CO ratios for the LSB.

H_2:CH_4 Sweeps at Constant $S_{L,0}$

In this section, $S_{T,LD}$ data acquired for H_2:CH_4 mixtures are reported. Again, data were acquired for mixtures where the H_2:CH_4 ratio and equivalence ratio were simultaneously adjusted to maintain the same mixture $S_{L,0}$ of 34 cm/s.

Figure 11 presents $S_{T,LD}$ as a function of u'_{ax} normalized by $S_{L,0}$ along with a correlation line found by Cheng et al. [4]. The results show reasonable agreement with the correlation. Note that the "fuel effect" is not as clearly present in this data as it was for the 12 mm Bunsen burner (Figure 2) and for the H_2:CO LSB data (Figure 10); for example, at $u'_{ax}/S_{L,0} \approx 7$, the $S_{T,LD}$ values increase starting with the 60:40 mixture, the 50:50 mixture, the pure CH_4, and, finally, the 50:50 mixture.

Figure 12 presents $S_{T,LD}$ as a function of u'_{ax} normalized by $S_{L,0}$ for all of the H_2:CO and H_2:CH_4 mixtures investigated. Note that the H_2:CO mixtures have generally higher $S_{T,LD}$ values than the H_2:CH_4 mixtures.

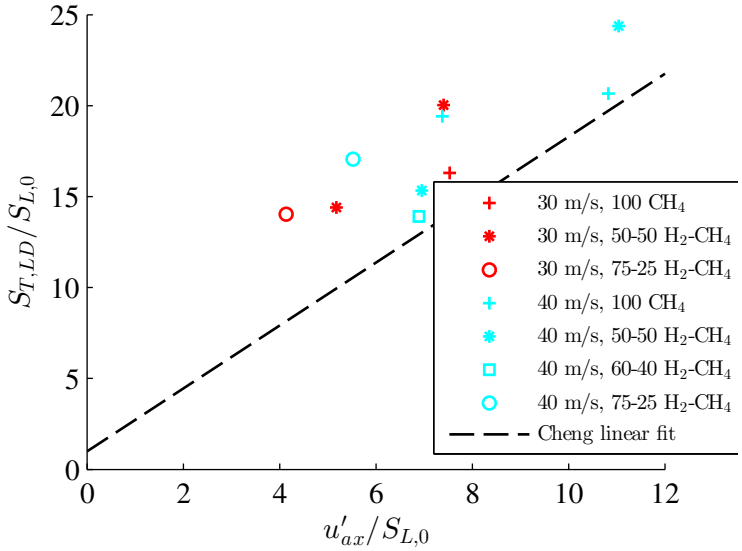

Figure 11: $S_{T,LD}$ as a function of u'_{ax} normalized by $S_{L,0}$ at various mean flow velocities and H_2:CH_4 ratios for the LSB.

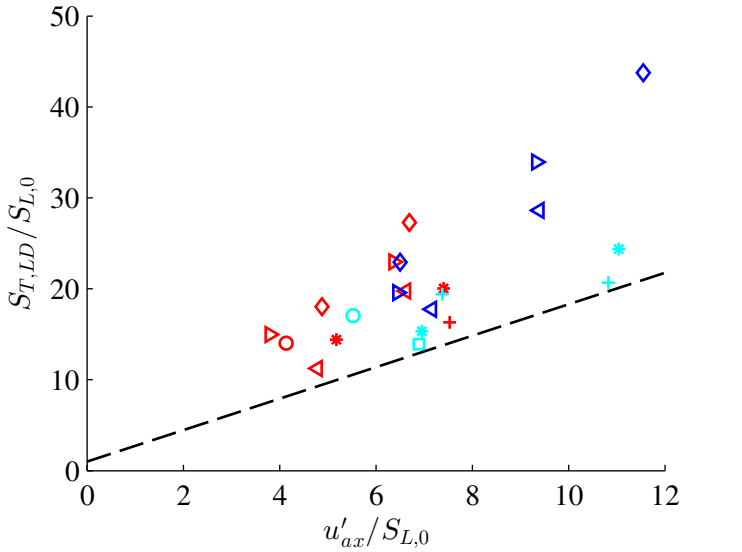

Figure 12: $S_{T,LD}$ as a function of u'_{ax} normalized by $S_{L,0}$ at various mean flow velocities for H_2:CO and H_2:CH_4 mixtures obtained in the LSB. See Figures 10 and 11 for legends.

Analysis

In this section, the data presented in Figure 12 are correlated using the steady-state leading points scaling law of Equation 1.

Figure 13 plots $S_{T,LD}$ as a function of u'_{ax} normalized by $S_{L,max}$. While the effects of this normalization are not as drastic as those observed with the Bunsen burner geometry, note that with the exception of the 50:50 H_2:CO points at $u'_{ax}/S_{L,0} = 1.4$ and 2, the data do tend to follow a clear trend-line.

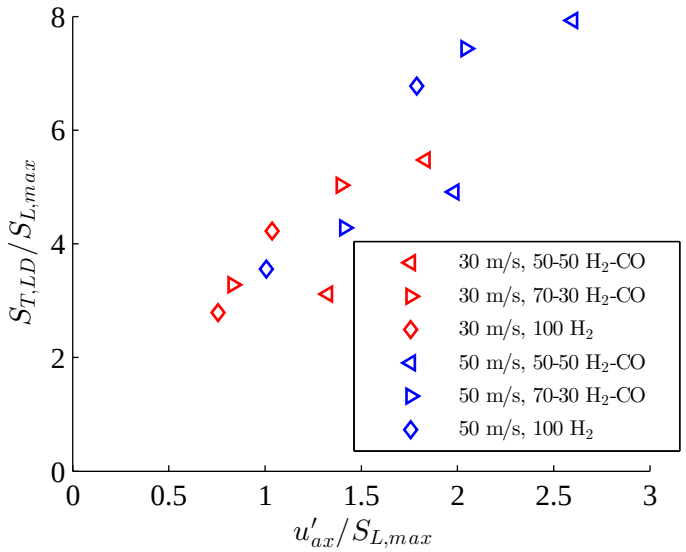

Figure 13: $S_{T,LD}$ as a function of u'_{ax} normalized by $S_{L,max}$ at various mean flow velocities and H_2:CO ratios for the LSB.

Figure 14 plots $S_{T,LD}$ as a function of u'_{ax} normalized by $S_{L,max}$. Note that although there was significant scatter in the data presented in Figure 11, when normalized instead with $S_{L,max}$ that the H_2:CH_4 data appear to collapse onto a single curve. This indicates that the data are well-correlated using the leading points model.

Finally, combining the two datasets onto one plot results in Figure 15. Note that while in Figure 12 the H_2:CO had consistently higher $S_{T,LD}$ values than the H_2:CH_4 mixtures, when normalized instead with $S_{L,max}$ that all the $S_{T,LD}$ data appear to collapse onto a single curve, indicating again that the leading points model performs well for this data.

Conclusions

In this report, we reported turbulent consumption speed measurements of H_2:CO blends from 1-10 atm and turbulent local displacement speed measurements for

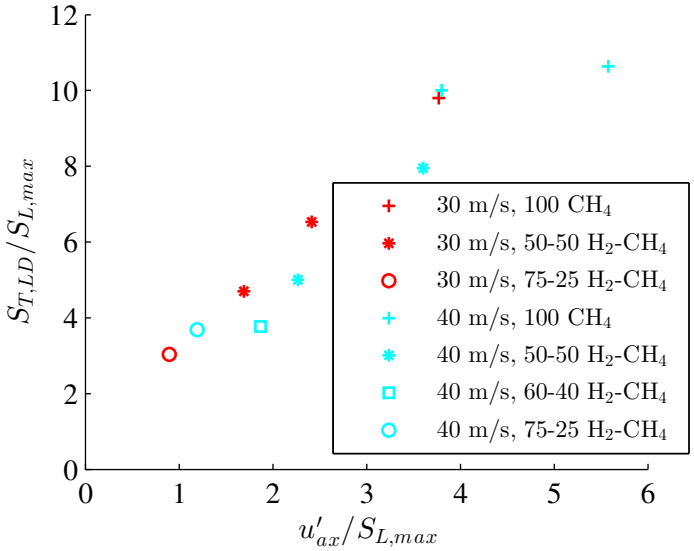

Figure 14: $S_{T,LD}$ as a function of u'_{ax} normalized by $S_{L,max}$ at various mean flow velocities and H_2:CH_4 ratios for the LSB.

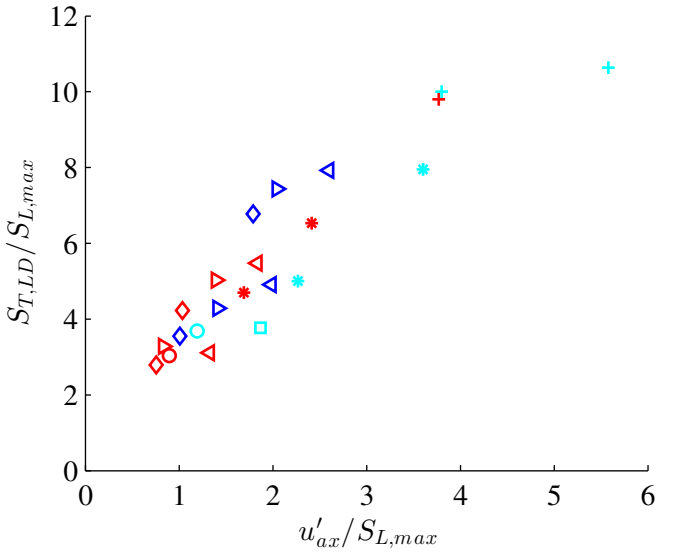

Figure 15: $S_{T,LD}$ as a function of u'_{ax} normalized by $S_{L,max}$ at various mean flow velocities for H_2:CO and H_2:CH_4 mixtures obtained in the LSB. See Figures 10 and 11 for legends.

H_2:CO and H_2:CH_4 mixtures. Experiments were conducted for mean flow velocities from 30-50 m/s for H_2:CO mixtures ranging from 50-100% H_2 by volume and H_2:CH_4 mixtures ranging from 0-75% H_2 by volume. For the consumption speed data it was found that at the same $S_{L,0}$ when the pressure was increased by a factor of 5, the consumption speed increased by almost a factor of 2. For the displacement speed data it was found that the H_2:CO mixtures exhibited clear "fuel effects" whereas the H_2:CH_4 mixtures did not appear to follow the same trends. It was also observed that the H_2:CO mixtures had generally higher $S_{T,LD}$ values than the H_2:CH_4 mixtures.

The data were then normalized with $S_{L,max}$. For the consumption speed data from the Bunsen burner, the data show that, at a given pressure, different fuel compositions and equivalence ratio data collapse. However, systematically different trends are observed with the 5 and 10 atm data. There is some evidence that these systematic differences are more fundamentally due to non-quasi-steady effects, as the pressure differences can be reasonably correlated with a computed chemical time scale for the 12 mm burner. For the displacement speed data acquired with the LSB, the leading points scaling model did an excellent job in collapsing the data over a very wide range of turbulence intensities and fuel compositions. This gives merit to the leading points model as a method that can be implemented across geometries and still produce meaningful results.

Bibliography

[1] A. Amato, M.S. Day, R.K. Cheng, J Bell, and T Lieuwen. Leading point statistics of a turbulent, lean, h2-air flame, April 2012.

[2] DR Ballal and AH Lefebvre. The structure and propagation of turbulent flames. *Proceedings of the Royal Society of London. A. Mathematical and Physical Sciences*, 344(1637):217–234, 1975.

[3] R. Borghi. On the structure and morphology of turbulent premixed flames. *Recent advances in the aerospace sciences(A 85-47304 23-31). New York, Plenum Press, 1985*, pages 117–138, 1985.

[4] R. K. Cheng, D. Littlejohn, P. A. Strakey, and T. Sidwell. Laboratory investigations of a low-swirl injector with h2 and ch4 at gas turbine conditions. *Proceedings of the Combustion Institute*, 32(2):3001–3009, 2009.

[5] G. Damköhler. The effect of turbulence on the flame velocity in gas mixtures. *Zeitschrift Electrochem*, 46:601–626, 1940.

[6] S. Daniele, P. Jansohn, J. Mantzaras, and K. Boulouchos. Turbulent flame speed for syngas at gas turbine relevant conditions. *Proceedings of the Combustion Institute*, 33(2):2937–2944, 2011.

[7] CJ Dasch. One-dimensional tomography: a comparison of abel, onion-peeling, and filtered backprojection methods. *Applied Optics*, 31(8):1146–1152, 1992.

[8] S. G. Davis, A. V. Joshi, H. Wang, and F. Egolfopoulos. An optimized kinetic model of h2/co combustion. *Proceedings of the Combustion Institute*, 30(1):1283–1292, 2005.

[9] F.N. Egolfopoulos. Geometric and radiation effects on steady and unsteady strained laminar flames. *Proceedings of the Combustion Institute*, 25(1):1375–1381, 1994.

[10] Hong G. Im and Jacqueline H. Chen. Effects of flow transients on the burning velocity of laminar hydrogen/air premixed flames. *Proceedings of the Combustion Institute*, 28(2):1833–1840, 2000.

[11] R.J. Kee, J.F. Grcar, MD Smooke, and JA Miller. Premix: a fortran program for modeling steady laminar one-dimensional premixed flames. Report SAND85-8240, Sandia National Laboratories, 1983.

[12] Robert J. Kee, James A. Miller, Gregory H. Evans, and Graham Dixon-Lewis. A computational model of the structure and extinction of strained, opposed flow, premixed methane-air flames. *Proceedings of the Combustion Institute*, 22(1):1479–1494, 1989.

[13] T Kitagawa, T Nakahara, K Maruyama, K Kado, A Hayakawa, and S Kobayashi. Turbulent burning velocity of hydrogen-air premixed propagating flames at elevated pressures. *International Journal of Hydrogen Energy*, 33(20):5842–5849, 2008.

[14] H. Kobayashi, T. Tamura, K. Maruta, T. Niioka, and F. A. Williams. Burning velocity of turbulent premixed flames in a high-pressure environment. *Proceedings of the Combustion Institute*, 26(1):389–396, 1996.

[15] W. Peiyong, S. Hu, J.A. Wehrmeyer, and R.W. Pitz. Stretch and curvature effects on flames, 2004.

[16] N. Peters. The turbulent burning velocity for large-scale and small-scale turbulence. *Journal of Fluid Mechanics*, 384:107–132, 1999.

[17] G. J. Smallwood, L. Glder, D. R. Snelling, B. M. Deschamps, and I. Gkalp. Characterization of flame front surfaces in turbulent premixed methane/air combustion. *Combustion and Flame*, 101(4):461–470, 1995.

[18] G. P. Smith, D. M. Golden, M. Frenklach, N. W. Moriarty, B. Eiteneer, M. Goldenberg, C. T. Bowman, R. K. Hanson, S. Song, W. C. Gardiner Jr, V. V. Lissianski, and Z. Qin. Gri-mech 3.0.

[19] P. Venkateswaran, A. Marshall, D. H. Shin, D. Noble, J. Seitzman, and T. Lieuwen. Measurements and analysis of turbulent consumption speeds of h2/co mixtures. *Combustion and Flame*, 158(8):1602–1614, 2011.

[20] Prabhakar Venkateswaran. *Measurements and Modeling of Turbulent Consumption Speeds of Syngas Fuel Blends*. PhD thesis, Georgia Institute of Technology, May 2013.

[21] C.K. Wu and C.K. Law. On the determination of laminar flame speeds from stretched flames. *Proceedings of the Combustion Institute*, 20(1):1941–1949, 1985.